Arch. Mech., 41, 4, pp. 461-480, Warszawa 1989

Elasto-plastic post-critical analysis of disks under tension

Z. MRÓZ and M. KOWALCZYK (WARSZAWA)

IN THE ELASTO-PLASTIC analysis of disks within the small strain theory, a continuous displacement solution may not exist and discontinuities in both velocity and displacement may occur within hyperbolic stress regimes or along transition lines between elliptic and hyperbolic regimes. To study elasto-plastic behaviour in the presence of discontinuity lines, it is assumed that an additional constitutive relation exists between displacement discontinuity and interface traction along a stationary discontinuity line. The general formulation is illustrated by a solution for an axisymmetric disk, using both Tresca and Huber–Mises yield conditions. It is demonstrated how the solution evolves from brittle to ductile response depending on disk thickness.

W analizie tarcz w zakresie sprężysto-plastycznym przy wykorzystaniu teorii małych odkształceń może nie istnieć ciągłe rozwiązanie opisujace rozkład przemieszczeń. Linie nieciągłości prędkości i przemieszczeń występują w stanach hiperbolicznych lub wzdłuż linii rozgraniczających eliptyczny i hiperboliczny stan naprężeń. W celu przeanalizowania sprężysto-plastycznego zachowania z liniami nieciągłości przyjęto założenie, że nieciągłość przemieszczeń i naprężenia normalne do linii nieciągłości związane są dodatkowym równaniem konstytutywnym. Ogólne sformułowanie zilustrowano na przykładzie rozwiązania tarczy osiowosymetrycznej z wykorzystaniem warunków Treski oraz Hubera–Misesa. Pokazano, w jaki sposób w zależności od grubości zachowanie tarczy zmienia się od kruchego do ciągliwego.

В анализе дисков в упруго-пластической области, при использовании теории малых деформаций, может не существовать непрерывное решение, описывающее распределение перемещений. Линии разрыва скорости и перемещений выступают в гиперболических состояниях или вдоль линий, разделяющих эллиптическое и гиперболическое состояния напряжений. С целью проанализирования упруго-пластического поведения с линиями разрыва принято предположение, что разрыв перемещений и нормальные напряжения к линии разрыва связаны дополнительным определяющим уравнением. Общая формулировка иллюстрирована на примере решения осесим-метричного диска с использованием условий Треска и Губера–Мизеса. Показано каким образом, в зависимости от толщины, поведение диска изменяется от хрупкого к тягучему.

1. Introduction

IN SOLVING boundary-value problems for elasto-plastic disks of a perfectly plastic material, different stress regimes are encountered, namely elliptic, hyperbolic or parabolic. For elliptic stress regimes, there are no real characteristics within the disk-plane, whereas for parabolic or hyperbolic regimes there exist one or two families of stress and velocity characteristics. Velocity discontinuities may then occur along characteristics as a part of the solution. Denoting by Δv_n and Δv_t the normal and tangential velocity discontinuities and by V_n the normal velocity of propagation of the material element across the discontinuity line S_v, the discontinuity in strain components referred to a local coordinate system (n, t) is expressed as follows:

$$\Delta \varepsilon_{nn} = \frac{\Delta v_n}{V_n}, \quad \Delta \gamma_{nt} = \frac{\Delta v_t}{V_n}, \quad \Delta \varepsilon_{tt} = 0, \tag{1.1}$$

where the n and t axes are normal and tangential to the line S_v.

From the relations (1.1) it follows that when the discontinuity line moves with the material particles ($V_n = 0$), the strain discontinuity tends to infinity. Such a situation occurs in axisymmetric disks which have stepwise varying thickness or are rigidly constrained at one of the edges. The solution for a rigid-plastic model then exhibits normal velocity discontinuity along circumferential lines (cf. [1, 2]) or normal displacement discontinuity in an elasto-plastic solution. Obviously, such a displacement or infinite strain discontinuity may create doubt about the physical validity of the solution. In a series of papers, K. SZUWALSKI and M. ŻYCZKOWSKI [3–9] introduced the concept of a decohesive capacity by assuming that velocity discontinuity on a stationary material line or surface is equivalent to local brittle decohesion.

In the present paper a different viewpoint is taken. It is assumed that an additional constitutive relation exists between the rate of displacement discontinuity and the respective traction rate along the material discontinuity line. On the other hand, the usual flow rule governs within domains of regular solution. Both geometric necking and material softening or hardening can be incorporated into the localized discontinuity mode. This general concept will be illustrated by solving an axisymmetric disk problem for both Tresca and Huber–Mises yield conditions and for a perfectly plastic material model. It turns out that the solution may exhibit both stable and unstable behaviour. A limit state is reached when total decohesion occurs on the discontinuity line and a full plastic regime develops within the disk. The present approach may be generalized to other cases and also to plates undergoing both flexure and extension, on the condition that proper constitutive relations are provided between rates of displacement discontinuities and the traction rates.

2. General solutions for elastic and elasto-plastic states

Consider an annular disk, uniformly loaded at its external boundary $r = b$ and rigidly supported at the interior boundary $r = a$ (Fig. 1). Before going into the details of the evolution of particular phases, we first present the general solutions in the elastic and elasto-plastic regimes taking into account the decohesive zone.

2.1. Elastic solution

Denote by $u(r, t)$ the radial displacement and by $\dot{u} = \dfrac{\partial u}{\partial \tau}$ its time rate of change. Within the small strain theory the strain components are specified as follows:

$$\varepsilon_r = \frac{\partial u}{\partial r}, \qquad \varepsilon_t = \frac{u}{r}. \tag{2.1}$$

As there are no body forces, the equilibrium equation is

$$\frac{\partial \sigma_r}{\partial r} + \frac{\sigma_r - \sigma_t}{r} = 0, \tag{2.2}$$

where $\sigma_r(r, t)$ and $\sigma_t(r, t)$ are radial and circumferential stresses. In writing Eq. (2.2) we neglect the thickness variation of the disk since Eq. (2.2) is valid for generalized stresses

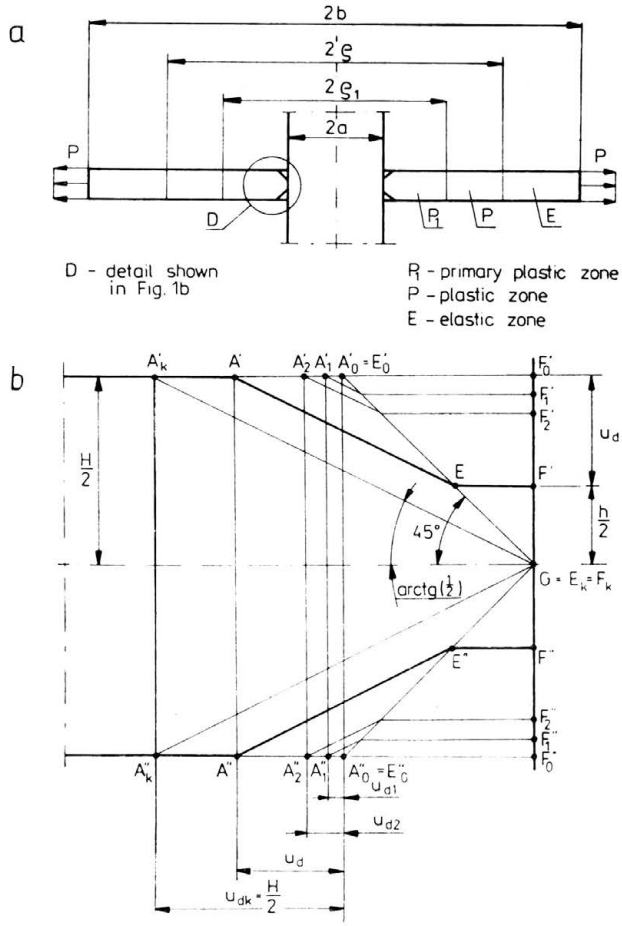

FIG. 1. a) Zones in the disk of elastic-perfectly plastic material. b) Mode of deformation in the localization zone.

$N_r = \sigma_r H$, $N_t = \sigma_t H$ (where H denotes the disk thickness and $\frac{H}{2} \ll a$). In subsequent analysis, the thickness variation will be considered only within a narrow decohesive zone in the vicinity of the edge $r = a$. Hooke's law provides the relations

$$\varepsilon_r = \frac{1}{E}(\sigma_r - \nu\sigma_t), \qquad \varepsilon_t = \frac{1}{E}(\sigma_t - \nu\sigma_r), \tag{2.3}$$

where E and ν are elastic constants. Solving the system (2.1)–(2.3) one obtains

$$\sigma_r = A_1 - A_2\frac{1}{r^2}, \qquad \sigma_t = A_1 + A_2\frac{1}{r^2},$$
$$u = \frac{1}{E}\left((1-\nu)A_1 r + (1+\nu)A_2\frac{1}{r}\right), \tag{2.4}$$

where A_1, A_2 are integration constants.

2.2. Elasto-plastic solution

Let us consider two yield conditions, namely Tresca (T) and Huber–Mises (HM), for which solutions will be discussed independently.

2.2.1. Tresca yield condition. In view of the equilibrium condition, the stress state $\sigma_r = \sigma_0$, $\sigma_t < \sigma_r$ represented by the side AB in Fig. 2 cannot exist. Hence the elasto-plastic state

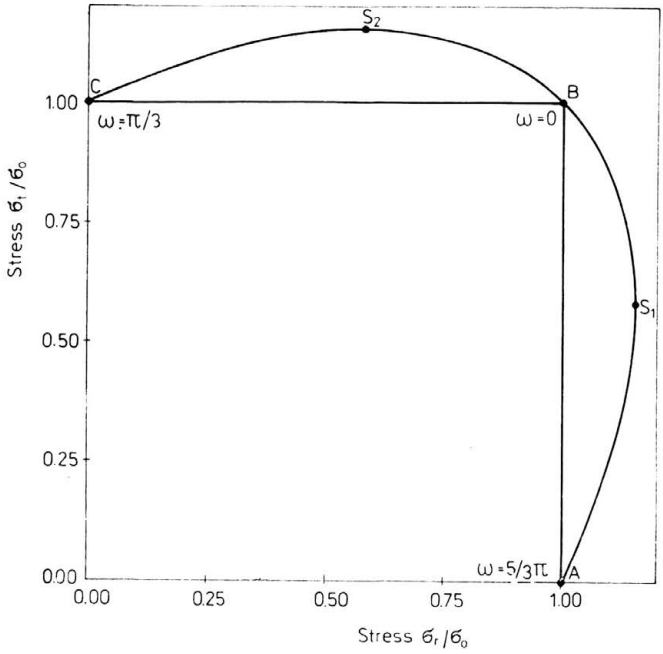

FIG. 2. Tresca and Huber–Mises yield surfaces.

should correspond to the side BC of the Tresca hexagon for wich $\sigma_t = \sigma_0$, $\sigma_r < \sigma_t$ (cf. Fig. 2). The equilibrium equation (2.2) then provides

$$\sigma_r = \sigma_0 + A_3 \frac{1}{r}, \qquad \sigma_t = \sigma_0, \tag{2.5}$$

where A_3 is an integration constant. The associated flow rule now provides

$$\begin{aligned} \dot{\varepsilon}_r &= \dot{\varepsilon}_r^e = \frac{1}{E}(\dot{\sigma}_r - \nu\dot{\sigma}_t), \\ \dot{\varepsilon}_t &= \dot{\varepsilon}_t^e + \dot{\varepsilon}_t^p = \frac{1}{E}(\dot{\sigma}_t - \nu\dot{\sigma}_r) + \dot{\lambda}\frac{\partial f}{\partial \sigma_t} = \frac{1}{E}(\dot{\sigma}_t - \nu\dot{\sigma}_r) + \dot{\lambda}. \end{aligned} \tag{2.6}$$

For progressing plastic flow, Eqs. (2.6) can be integrated to yield

$$\varepsilon_r = \varepsilon_r^e, \qquad \varepsilon_t = \varepsilon_t^e + \lambda, \qquad \lambda = \varepsilon_t^p \tag{2.7}$$

and, in view of Eqs. (2.3) and (2.5), we obtain

$$u = \frac{1}{E}\left((1-\nu)\sigma_0 r + A_3(\ln r - \nu) + A_4\right) \tag{2.8}$$

with a new integration constant A_4.

2.2.2. Huber-Mises yield condition. The Huber–Mises yield condition is satisfied by using the stress representation

$$\sigma_r = \frac{2}{\sqrt{3}}\sigma_0 \cos\left(\omega + \frac{\pi}{6}\right), \qquad \sigma_t = \frac{2}{\sqrt{3}}\sigma_0 \cos\left(\omega - \frac{\pi}{6}\right), \tag{2.9}$$

where ω is a stress parameter specifying a stress point on the Huber–Mises ellipse (cf. Fig. 2).

$$f = \sigma_r^2 + \sigma_{tt}^2 - \sigma_r\sigma_t - \sigma_0^2 = 0. \tag{2.10}$$

The stress field is therefore specified by providing a function $\omega = \omega(r, t)$. From Eqs. (2.2) and (2.9), one obtains

$$r = A_3\left(e^{\sqrt{3}\omega}\sin\omega\right)^{-0.5} \tag{2.11}$$

with the constant A_3 to be determined from a boundary condition. This stress distribution occurs within a plastic zone developing from the interior edge before the decohesive process initiates. This initiation starts once the stress path reaches the parabolic point S_1 (cf. Fig. 2). It can be expected that the primary plastic zone is small, as was shown in [4]. Therefore, when using the Hencky–Ilyushin deformation theory, this primary zone was neglected in [4] and the secondary plastic zone developing after the decohesion process was taken into account.

Let us present briefly the formulation of the deformation theory and specify the displacement field associated with the relation (2.11). We have

$$\frac{\varepsilon_r - \varepsilon_m}{\varepsilon_t - \varepsilon_m} = \frac{2\sigma_r - \sigma_t}{2\sigma_t - \sigma_r}, \qquad \varepsilon_m = \frac{\sigma_r + \sigma_t}{9K}, \tag{2.12}$$

where $K = E/3(1-2\nu)$ is the bulk modulus and ε_m denotes the mean volumetric strain. Using the compatibility condition

$$\frac{\partial}{\partial r}(r\varepsilon_t) = \varepsilon_r, \tag{2.13}$$

the following differential equation is obtained from Eqs. (2.9), (2.12) and (2.13):

$$\frac{\partial \varepsilon_t}{\partial \omega} - \sqrt{3}\,\varepsilon_t = \frac{2\sigma_0}{3K\sqrt{3}}\cos\omega \tag{2.14}$$

from which it follows that

$$\varepsilon_t = \frac{\sigma_0}{3K\sqrt{3}}\cos\left(\omega + \frac{\pi}{6}\right) + A_4 e^{\sqrt{3}\omega}. \tag{2.15}$$

The displacement field is obtained from Eqs. (2.15) and (2.11), namely

$$u = \frac{A_3\sigma_0}{3K\sqrt{3}}\cos\left(\omega+\frac{\pi}{6}\right)\left(e^{\sqrt{3}\,\omega}\sin\omega\right)^{-0.5} + A_3A_4\left(\frac{e^{\sqrt{3}\,\omega}}{\sin\omega}\right)^{0.5} \tag{2.16}$$

with the constants A_3, A_4 to be specified from the boundary or continuity conditions.

When the associated flow rule is used, the strain and stress rates are related by

$$\left(\dot{\varepsilon}_r-\frac{1}{E}(\dot{\sigma}_r-\nu\dot{\sigma}_t)\right)(2\sigma_t-\sigma_r) = \left(\dot{\varepsilon}_t-\frac{1}{E}(\dot{\sigma}_t-\nu\dot{\sigma}_r)\right)(2\sigma_r-\sigma_t) \tag{2.17}$$

which results in the following equation for $\dot{\varepsilon}_t$:

$$\frac{\partial\dot{\varepsilon}_t}{\partial\omega}-\sqrt{3}\,\dot{\varepsilon}_t = \frac{2\sigma_0\dot{\omega}}{\sqrt{3}}\left(\frac{1}{4G\sin\omega}+\frac{\sin\omega}{3K}\right), \tag{2.18}$$

where $G = E/2(1+\nu)$ is the shear modulus. The solution of this equation will be obtained numerically. In view of the relation (2.11), Eq. (2.18) can also be presented in the form

$$\frac{\partial\dot{\varepsilon}_t}{\partial r} = -\left[\frac{2\sigma_0\dot{\omega}}{\sqrt{3}}\left(\frac{1}{4G}+\frac{\sin^2\omega}{3K}\right)+\sqrt{3}\,\dot{\varepsilon}_t\sin\omega\right]\left(r\cos\left(\omega-\frac{\pi}{6}\right)\right)^{-1}. \tag{2.19}$$

2.3. Decohesive zone

For the Tresca material an elasto-plastic solution satisfying the condition $u = 0$ at $r = a$ does not exist since the stress state in the plastic regime must correspond to the side BC for which $f_2 = \sigma_t-\sigma_0 = 0$. When the first plastic flow occurs at $r = a$ and for the side AB $\sigma_r = \sigma_0$, $\sigma_t < \sigma_0$, at the subsequent instant we must have $\sigma_r = \sigma_t = \sigma_0$ at $r = a$ since the final plastic zone corresponding to the side AB cannot exist. The elasto-plastic solution can only be constructed by assuming the displacement discontinuity $u = u_d$ at $r = a$.

On the other hand, for the Huber–Mises yield condition a continuous elasto-plastic solution for a compressible material ($\nu < 0.5$) can be constructed with the respective displacement field satisfying $u = 0$ at $r = a$. A primary plastic zone will first develop at the interior edge $r = a$. When the stress point representing the stress state in the plane $\sigma_r-\sigma_t$ for $r = a$ approaches the parabolic point S_1 (cf. Fig. 2), the radial strain $\varepsilon_r(a)$ increases rapidly, tending to infinity when $\sigma_t(a) = 0.5\sigma_r(a)$. This means that a regular elasto-plastic solution no longer exists. For the case $\nu = 0.5$, the parabolic point is reached by the elastic stress path (cf. [4]).

Physically it can be expected that a localized flow zone (or decohesive zone) occurs near the edge $r = a$. Denote the stress for $r = a$ at the onset of decohesion by $\sigma_r^*(a)$ and $\sigma_t^*(a)$. Our analysis is based on a simplified description of this zone starting from the following assumptions.

For simplicity, assume that the axisymmetric stress state is approximated by the plane strain state occurring within the plane r, z. Moreover, it is assumed that the localization process develops within the zone $a \leqslant r \leqslant a+\frac{H}{2}$. The stress state is assumed as uniform in this zone([1]).

([1]) This approximation is discussed in more detail in the appendix.

Figure 1b presents the mode of deformation in the localization zone. The slip surfaces GE' and GE'' are inclined at $\pi/4$ with respect to the middle disk plane. Two rigid material portions $GE'F'$ and $GE''F''$ are sliding along slip planes toward this plane, thus inducing local thickness reduction. The cross section $A'A''$ of constant thickness is displaced by u_d. It is seen that the reduced thickness h is related to u_d, $h = H-2u_d$. The stress state $\sigma_r^*(a)$, $\sigma_t^*(a)$ is uniform in the decohesive zone. Thus the stress states in the cross sections $F'F''$ and $E'E''$ are the same, whereas the radial stress in the cross section $A'A''$ follows from the condition of equilibrium of radial disk forces, so that

$$\begin{aligned} &\sigma_r(A'A'') = \sigma_r^*(a)\left(1-2\frac{u_d}{H}\right), && u_d < \frac{H}{2}, \\ &\sigma_r(A'A'') = 0, && u_d \geqslant \frac{H}{2}. \end{aligned} \tag{2.20}$$

Further, we assume that the cross section $A'A''$ constitutes an "edge" for the remaining disk portion where a regular solution exists; thus the boundary conditions for this solution are specified in the form

$$\begin{aligned} \sigma_r(a) &= \sigma_r(A'A''), \\ u(a) &= u_d. \end{aligned} \tag{2.21}$$

As it follows from Eqs. (2.20) the radial stresses (2.21) at the disk edge constituting the boundary stresses for a regular solution will diminish to zero in the course of the decohesion process. Thus local unloading occurs near the interior edge.

We now discuss the details of the solution for this new boundary-value problem.

3. Elasto-plastic solution taking into account the decohesive zone

In this section, we shall discuss the details of the elasto-plastic solution taking into account the softening zone at $r = a$ due to localized plastic flow.

3.1. Elastic solution

Within the elastic regime, the boundary conditions

$$u(a) = 0, \quad \sigma_r(b) = \mathrm{p} \tag{3.1}$$

are sufficient to specify the elastic solution (2.4). The integration constants follow from the conditions (3.1), namely

$$A_1 = \frac{(1+\nu)pb^2}{(1+\nu)b^2+(1-\nu)a^2}, \quad A_2 = \frac{-(1-\nu)pa^2b^2}{(1+\nu)b^2+(1-\nu)a^2}. \tag{3.2}$$

The elastic solution ceases its validity when the stress state at $r = a$ reaches the yield surface. The value of p corresponding to the onset of plastic flow is given as follows:

Tresca yield condition

$$p_T = \frac{\sigma_0}{2b^2}\left((1+\nu)b^2+(1-\nu)a^2\right), \tag{3.3}_1$$

Huber–Mises yield condition

$$(3.3)_2 \qquad p_{HM} = \frac{\sigma_0}{2\sqrt{1-\nu+\nu^2}\, b^2}\left((1+\nu)b^2+(1-\nu)a^2\right).$$

3.2. Elastic solution with the decohesive zone

For the Tresca yield condition or for the deformation theory (2.12), we assume that when Eq. (3.3) is satisfied, the subsequent plastic flow is localized in the cohesive zone near the edge $r = a$, so that the displacement discontinuity $u_d(a)$ satisfies the softening condition (2.20). Setting

$$(3.4) \qquad \sigma^*_{r_+}(a) = \sigma_0$$

for the Tresca material and

$$(3.5) \qquad \sigma^*_r(a) = \frac{\sigma_0}{\sqrt{1-\nu+\nu^2}}$$

for the Huber–Mises material, the constants A_1, A_2 can be determined from the relations (2.20), (2.21) and the condition $\sigma_r(b) = p$. We obtain

$$(3.6) \qquad \begin{aligned} A_1 &= \frac{1}{2}\left(E\frac{u_d}{a}+(1+\nu)\sigma^*_r(a)\left(1-2\frac{u_d}{H}\right)\right), \\ A_2 &= \frac{a^2}{2}\left(E\frac{u_d}{a}-(1-\nu)\sigma^*_r(a)\left(1-2\frac{u_d}{H}\right)\right). \end{aligned}$$

In the course of growth of u_d, the radial stress decreases in the vicinity of $r = a$ and the circumferential stress increases. A plastic zone may occur near the internal edge before the decohesive process ends, or the decohesive process may end first and full separation between the disk and the hub then occurs.

3.3. Elasto-plastic solution with the decohesive zone

Consider the case when the plastic zone starts to develop first. The constants A_1, A_2, A_3, A_4 occurring in Eqs. (2.4), (2.5), (2.8) or (2.11), (2.16) and the radius ϱ of the plastic zone are determined from the conditions (2.20), (2.21), the condition $\sigma_r(b) = p$ and the continuity conditions at $r = \varrho$: $u^e(\varrho) = u^p(\varrho)$, $\sigma^e_r(\varrho) = \sigma^p_r(\varrho)$ where e and p denote elastic and plastic solutions respectively. Moreover, the yield condition should be satisfied by the elastic solution at $r = \varrho$, thus $\sigma^e_t(\varrho) = \sigma^p_t(\varrho)$. The integration constants now become

Tresca yield condition

$$(3.7) \qquad \begin{aligned} A_1 &= \frac{1}{2}\left(E\frac{u^p(\varrho)}{\varrho}+(1+\nu)\sigma^p_r(\varrho)\right), \\ A_2 &= \frac{\varrho^2}{2}\left(E\frac{u^p(\varrho)}{\varrho}-(1-\nu)\sigma^p_r(\varrho)\right), \end{aligned}$$

$$A_3 = -2\sigma_0 \frac{au_d}{H},$$

$$A_4 = Eu_d - (1-\nu)\sigma_0 a + 2\sigma_0 \frac{au_d}{H}(\ln a - \nu).$$

The end of this phase occurs when the decohesive process ends ($u_d > 0.5H$) or the whole disk becomes plastic.

Consider now the case when the disk becomes plastic before the termination of the decohesive process. Then only A_3, and A_4 occur in the solution. They are determined from the relations (2.20), (2.21) and the condition $\sigma_r(b) = p$. For the Tresca material, we obtain

$$A_3 = -2\sigma_0 \frac{au_d}{H},$$

(3.8)

$$A_4 = Eu_d - (1-\nu)\sigma_0 a + 2\sigma_0 \frac{au_d}{H}(\ln a - \nu).$$

The process terminates when total decohesion occurs ($u_d = 0.5H$) and the disk passes into the limit state.

We see that various sequences of development of different phases of deformation can occur there. They depend on the geometric parameters of the disk, that is, ratios b/a and a/H.

3.4. Numerical elasto-plastic solution for the flow rule (2.17)

The incremental numerical procedure is applied for the case of the Huber–Mises yield condition and the associated flow rule. The primary plastic zone P_1 ($a \leqslant r \leqslant \varrho_1$), for which $\sigma_r > \sigma_t$, $\dot{\varepsilon}_t^p < 0$, develops near the edge $r = a$. The stress and displacement fields are calculated in this zone by integrating Eq. 2.19 numerically, which can be rewritten in the form

$$\frac{\partial(\Delta\varepsilon_{ti})}{\partial r} = -\left[\frac{2(\Delta\omega_i)\sigma_0}{\sqrt{3}}\left(\frac{1}{4G} + \frac{\sin^2\omega}{3K}\right) + \sqrt{3}(\Delta\varepsilon_{ti})\sin\omega\right]\left(r\cos\left(\omega - \frac{\pi}{3}\right)\right)^{-1}, \tag{3.9}$$

where $\Delta\varepsilon_{ti}$ and $\Delta\omega_i$ are increments of ε_t and ω at the consecutive integration step. This equation can be integrated within the plastic zone $a \leqslant r \leqslant \varrho_1$ using the explicit Eulerian scheme. Next, the displacement increment Δu_i can be calculated, and the elastic solution in the domain $\varrho_1 \leqslant r \leqslant b$ is updated accordingly. When $\varepsilon_t(a)$ tends to large values, it indicates that the decohesive process starts and the stress point approaches the parabolic point S_1. Next, decohesive deformation develops and, consequently, elastic unloading occurs near the disk edge. The secondary plastic flow within zone P_2 occurs for $\sigma_t > \sigma_r$, $\dot{\varepsilon}_t^p > 0$ with the plastic zone spreading from the edge $r = a$. If the decohesive process ends first, the calculation is continued until the whole disk becomes plastic.

4. Examples

A set of examples was solved for both Tresca and Hubert–Mises yield conditions associated with the deformation or flow theories. Table 1 presents the material constants

Table 1.

Data set	1	2	3	4	5	6	7	8	9	10	11
σ_0/E	.001	.001	.001	.001	.001	.001	.001	.0015	.001	.001	.001
ν	0.3	0.3	0.3	0.3	0.3	0.2	0.4	0.3	0.3	0.3	0.3
b/a	4.	4.	4.	4.	4.	4.	4.	4.	2.	6.	8.
a/H	400.	300.	250.	200.	100.	250.	250.	250.	400.	400.	400.

Table 2.

Data set		1		2			3	4	5	6	7	8	9	10	11
Yield condition		T	HM	T	HM	HM	HM	T	T	HM	HM	HM	T	T	T
Theory		PR	HI	PR	HI	PR	HI	PR	PR	HI	HI	HI	PR	PR	PR
Phase	1	E ↗	E ↗	E ↗	E ↗	E ↗	E ↗	E ↗	E ↗	E ↗	E ↗	E ↗	E ↗	E ↗	E ↗
	2	DE ↘	DE ↘	DE ↗	DE ↗	P_1E ↗	DE ↗	DE ↗	DE ↗	DE ↗	DE ↗	DE ↘	DE ↘	DE ↘	DE ↘
	3	DPE ↘	DPE ↘	DPE ↘	DPE ↘	DP_1E →	DPE ↘	DPE ↘	DPE ↘	DPE ↘	DPE ↘	DPE ↙	DPE ↘	DPE ↙	DPE ↙
	4	PE ↗	PE ↗	PE ↗	PE ↗	DP_2P_1E ↗	PE ↗	DP ↘	DP ↘	PE ↗	PE ↗	PE ↗	PE ↗	PE ↗	PE ↗
	5	P →	P →	P →	P →	DP_1P_2E ↗	P →	P →	P →	P →	P →	P →	P →	P →	P →
	6	—	—	—	—	DP_1P_2 ↘	—	—	—	—	—	—	—	—	—
	7	—	—	—	—	P_1P_2 →	—	—	—	—	—	—	—	—	—

T — Tresca yield condition
HM — Huber–Mises yield condition
PR — flow theory
HI — deformation theory
D — decohesive zone
↗ — stable process
E — elastic zone
↘ — unstable process, displacement controllable
P — plastic zone
P_1 — primary plastic zone
↙ — unstable process, uncontrollable
P_2 — secondary plastic zone
→ — constant load

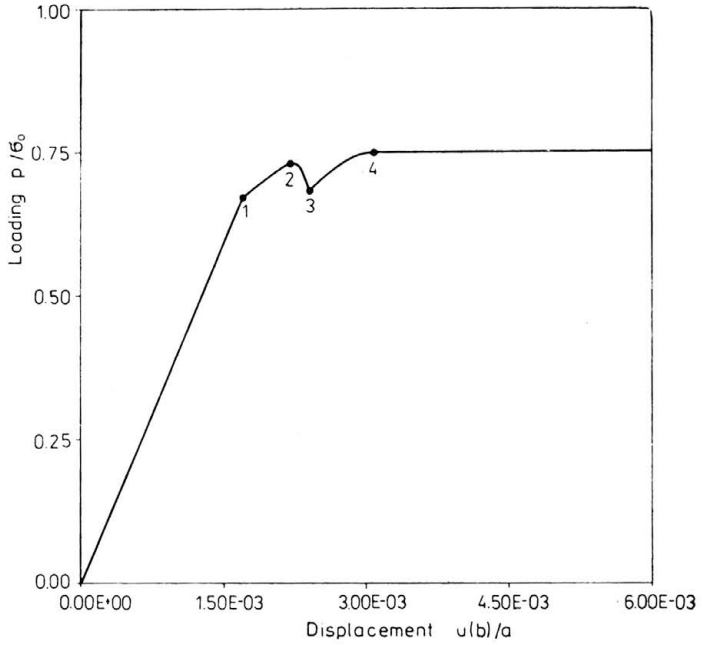

FIG. 3. Relation between loading p/σ_0 and displacement of the disk edge $r = b$ for particular phases of deformation, for the Tresca yield condition and the associated flow rule. Disk parameters: $b/a = 4$, $a/H = 300$, $\nu = 0.3$, $\sigma_0/E = 0.001$. *1–2* elastic deformation with decohesion, *2–3* elasto-plastic deformation with decohesion, *3–4* elasto-plastic deformation after decohesion.

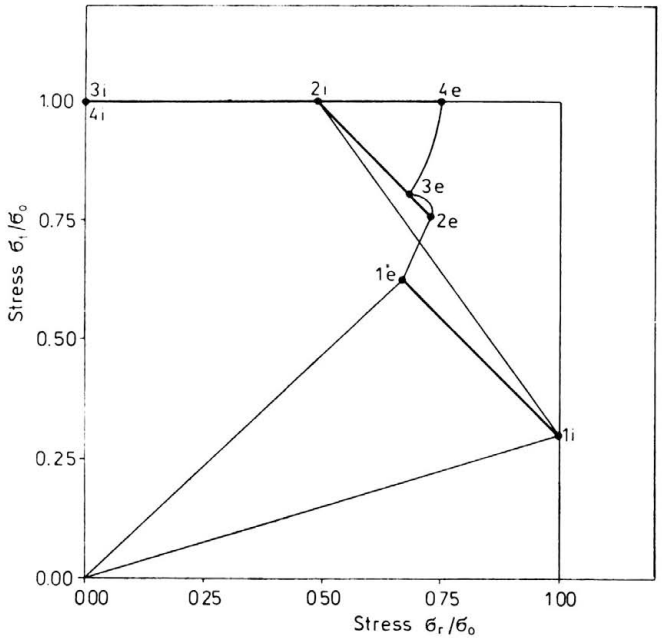

FIG. 4. Evolution of the stress state within disk for Tresca yield condition and the associated flow rule. Disk parameters: $b/a = 4$, $a/H = 300$, $\nu = 0.3$, $\sigma_0/E = 0.001$. i — points representing stress states on the interior edge $r = a$, e — points representing stress states on the exterior edge $r = b$.

and geometric parameters used in the particular examples. Table 2 presents the sequence of development of particular regimes within the disks considered.

Figure 3 presents the dependence of the external loading p/σ_0 on the displacement of the loaded disk edge $r = b$ for the parameters $b/a = 4$, $a/H = 300$, $\nu = 0.3$, $\sigma_0/E = 0.001$. The results correspond to the Tresca yield condition and the associated flow rule. It is seen that the elastic phase with decohesion corresponds to stable behaviour. However, the elasto-plastic phase with decohesion is unstable, and the quasi-static deformation process should occur under displacement control. After total decohesion ($\sigma_r(a) = 0$, $u_d > 0.5H$), the subsequent development of the plastic zone is stable until limit state 4 is reached. Figure 4 presents the evolution of the stress state within the disk at consecutive stages. The interior edge first becomes plastic when the stress point i reaches the side AB: $\sigma_r = \sigma_0$, $\sigma_t < \sigma_0$. However, when the decohesion process develops, elastic unloading occurs in the vicinity of the edge $r = a$, and subsequently the material becomes plastic at the state represented by the side BC: $\sigma_t = \sigma_0$, $\sigma_r < \sigma_0$. During decohesion, the stress point at $r = a$ moves to C and total decohesion occurs.

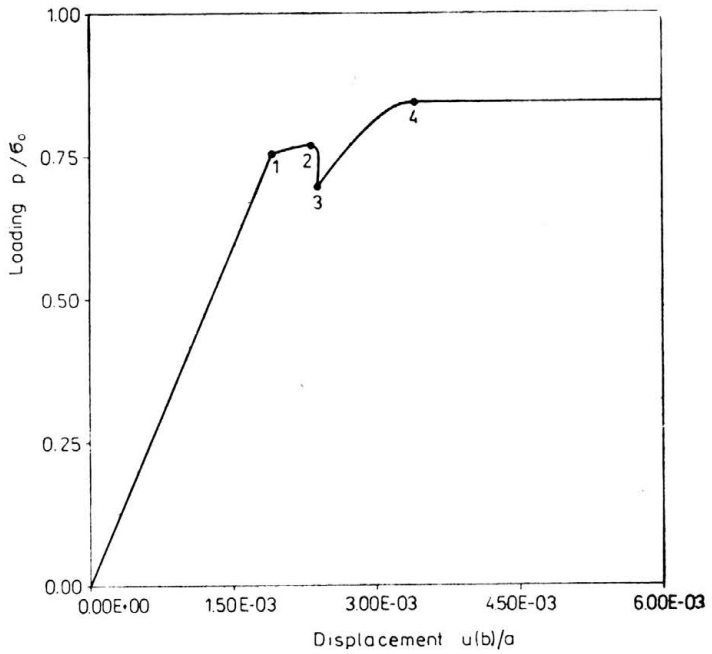

FIG. 5. Relation between disk loading p/σ_0 and edge displacement for the Huber–Mises yield condition and the deformation theory. Disk parameters: $b/a = 4$, $a/H = 300$, $\nu = 0.3$, $\sigma_0/E = 0.001$. *1–2* elastic deformation with decohesion, *2–3* elasto-plastic deformation with decohesion, *3–4* elasto-plastic deformation after decohesion.

Figure 5 presents the load-deflection curve for the same disk parameters but for the Huber–Mises yield condition and the deformation theory. Similarly as in [4], the plastic flow prior to decohesion was neglected, and hence the sequence of phases is the same as in Fig. 4. Figure 6 shows the respective stress evolution for the Huber–Mises yield

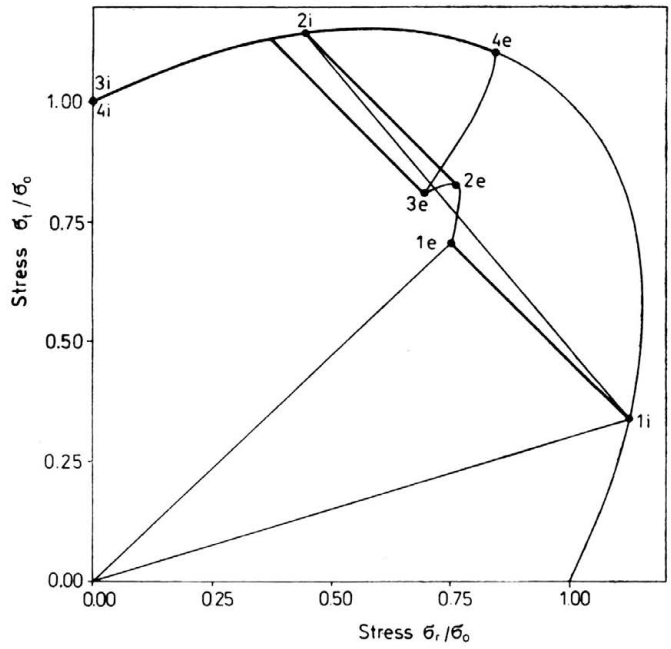

FIG. 6. Evolution of the stress state within the disk for the Huber–Mises yield condition and the deformation theory. Disk parameters: $b/a = 4$, $a/H = 300$, $\nu = 0.3$, $\sigma_0/E = 0.001$, i — points representing stress states on the interior edge $r = a$, e — points representing stress states on the exterior edge $r = b$.

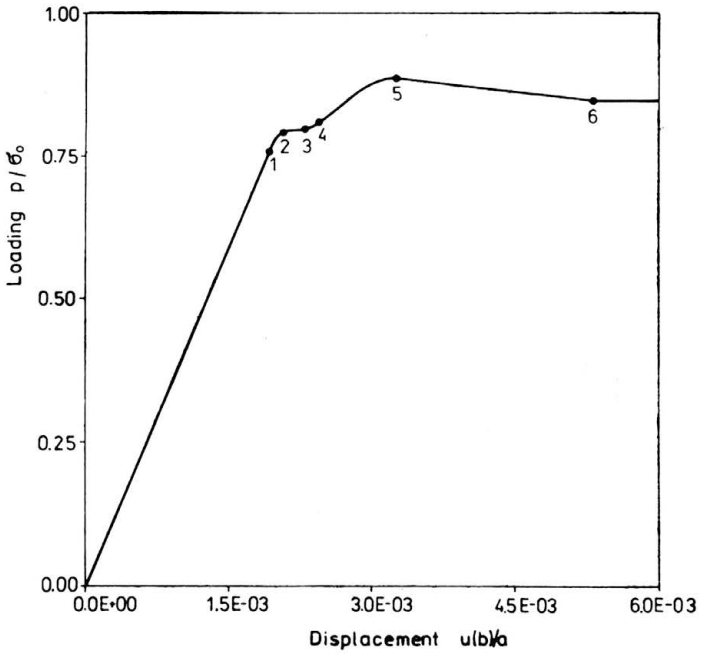

FIG. 7. Relation between disk loading p/σ_0 and edge displacement for the Huber–Mises yield condition and the associated flow rule. Disk parameters: $b/a = 4$, $a/H = 300$, $\nu = 0.3$, $\sigma_0/E = 0.001$. *1–2* phase of primary plastic flow within the zone $a < r < \varrho_1$, *2–3* phase of elastic unloading with decohesion, *3–4* phase of secondary plastic flow within the zone $a < r < \varrho_1$ with decohesion, *4–5* phase of plastic flow, $\varrho > \varrho_1$, with decohesion, *5–6* phase of decohesion after total plastic flow.

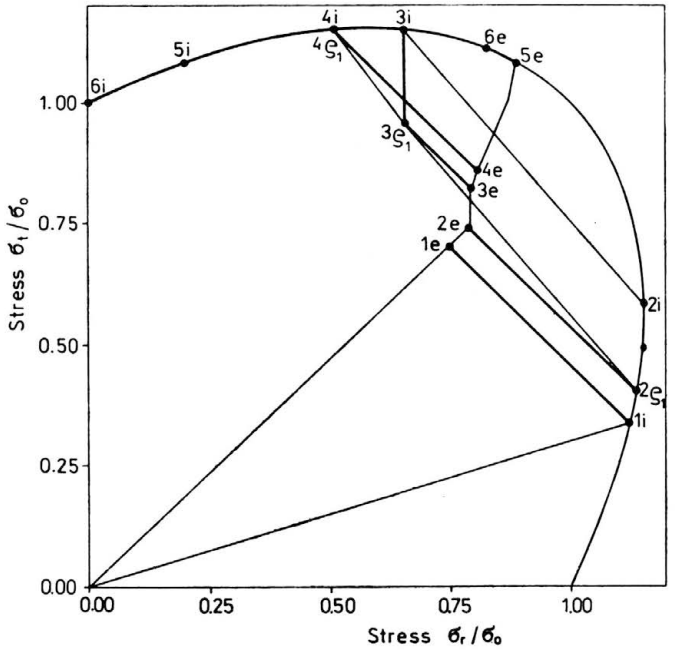

FIG. 8. Stress evolution in the disk during consecutive phases for the Huber–Mises yield condition and the associated flow rule. Disk parameters: $b/a = 4$, $a/H = 300$, $\nu = 0.3$, $\sigma_0/E = 0.001$. i — points representing stress states on the interior edge $r = a$, e — points representing stress states on the exterior edge $r = b$, ϱ_1 — points representing stress states at the interface between elastic and primary plastic zones.

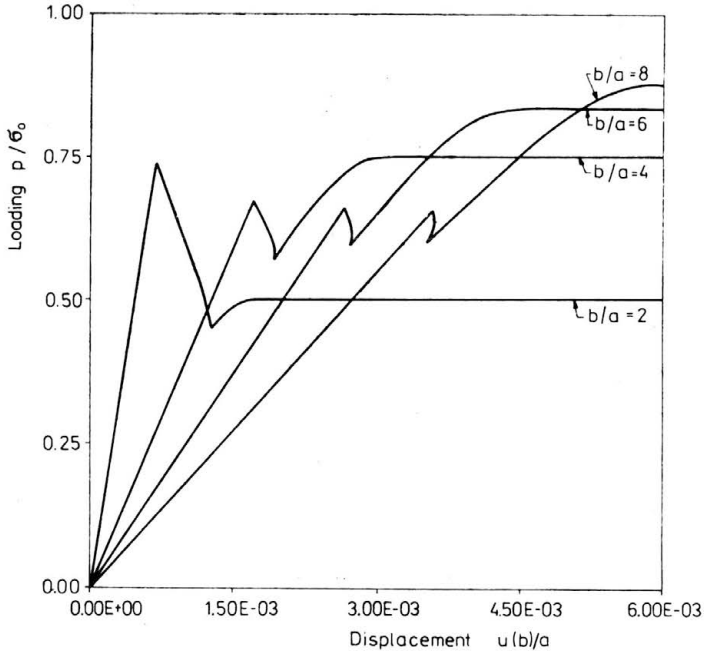

FIG. 9. Effect of the external disk radius on load-displacement curves for the Tresca yield condition and the associated flow rule.
Disk parameters: $a/H = 400$, $\nu = 0.3$, $\sigma_0/E = 0.001$.

condition and the deformation theory. It is seen that both the Tresca yield condition with the associated flow rule and the deformation theory demonstrate similar behaviour, as there is no effect of plastic flow preceding the decohesion process.

Figures 7 and 8 present the solution of the same case but for the Huber–Mises yield condition and associated flow rule taking into account the plastic zone P_1 developing before the initiation of decohesion. It is seen that the load-displacement curve does not exhibit an unstable portion that was predicted for the Tresca yield condition or the deformation theory. The segment 1–2 in Fig. 7 corresponds to the development of the primary plastic zone, with the stress point representing the edge stress moving from $1i$ to $2i$ in Fig. 8. The radial strain increases rapidly when $2i$ reaches the parabolic point S_1, and next the decohesion process starts to develop. The decohesion process induces unloading in the vicinity of the interior edge and during the phase 2–3 the interior stress point again reaches the yield surface at $3i$ (Fig. 8). Note that at $3i$ we have $\dot{\varepsilon}_r^p > 0$, $\dot{\varepsilon}_t^p > 0$, that is, $3i$ corresponds to the elliptic regime. During the phase 3–4 the secondary plastic zone spreads, so at $4i$ it is equal to the primary plastic zone. Moreover, the stress solution passes through the parabolic point S_2 and enters into the hyperbolic regime for which $\dot{\varepsilon}_r^p < 0$, $\dot{\varepsilon}_t^p > 0$. Further decohesion induces translation of the edge stress point to $5i$ and $6i$ for which $\sigma_r(a) = 0$. At stage 5 the whole disk becomes plastic and the phase 5–6 corresponds to decohesion plastic flow of the whole disk. In Fig. 8, the stress is shown at the point ϱ_1 corresponding to the interface reached at the end of primary plastic flow. Due to the complex history of plastic flow, the instability is exhibited only during the phase 5–6. Note also that the

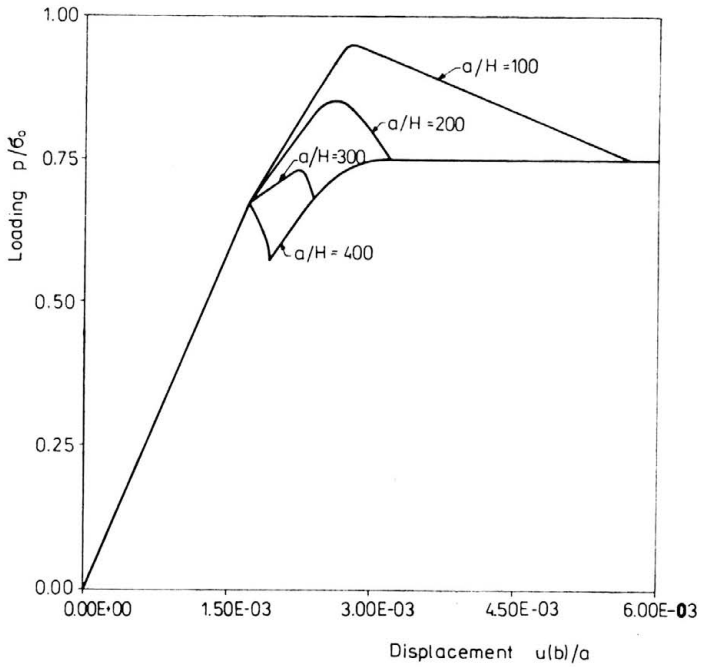

FIG. 10. Effect of the disk thickness on load-displacement curves for the Tresca yield condition and the associated flow rule.
Disk parameters: $b/a = 4$, $\nu = 0.3$, $\sigma_0/E = 0.001$.

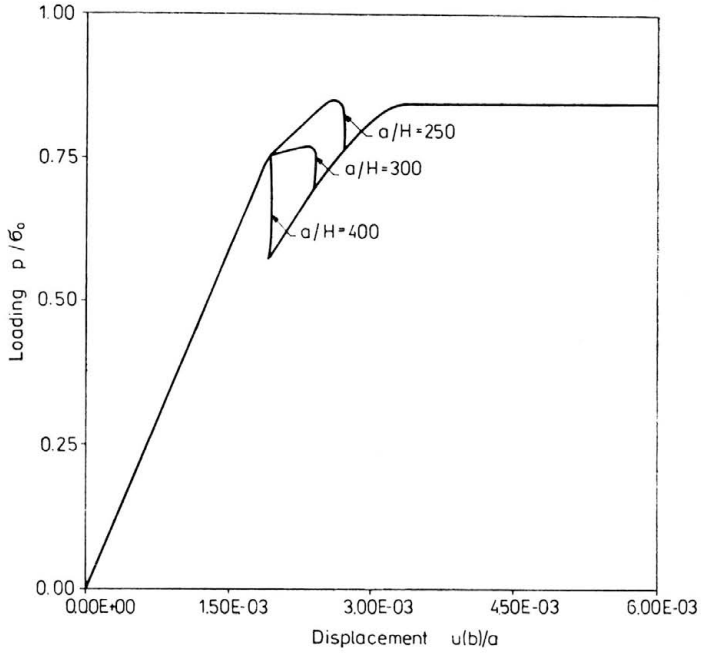

FIG. 11. Effect of the disk thickness on load-displacement curves for the Huber–Mises yield condition and the deformation theory.
Disk parameters: $b/a = 4$, $\nu = 0.3$, $\sigma_0/E = 0.001$.

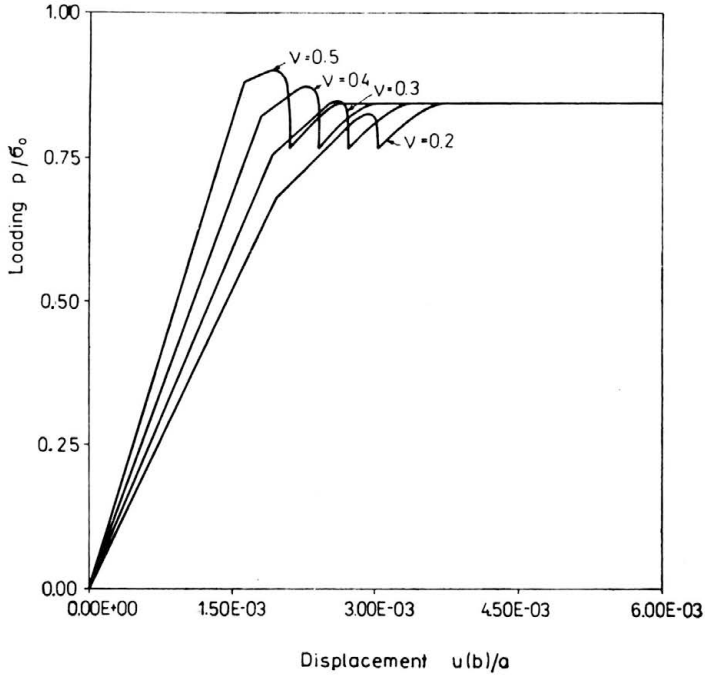

FIG. 12. Effect of Poisson's ratio on load-displacement curves for the Huber–Mises yield condition and the deformation theory.
Disk parameters: $b/a = 4$, $a/H = 250$, $\sigma_0/E = 0.001$.

sequence of phases is now different since the decohesion process continues during the whole period of deformation and full plastic flow of the disk precedes the end of the decohesion process.

Figure 9 presents the effect of external disk radius on the load-displacement curves. It is seen that for $b/a > 2$, the load-displacement curve not only exhibits unstable, displacement controllable portions ($\dot{p} < 0$, $\dot{u}(b) > 0$), but also unstable and uncontrollable portions ($\dot{p} < 0$, $\dot{u}(b) < 0$). Further, the onset of decohesion does not correspond to maximal load: for larger values of b/a the limit load is usually higher than the load associated with the onset of decohesion. Figures 10 and 11 present the effect of disk thickness. As expected, thicker disks exhibit more ductile behaviour and a very short transition to the limit states, whereas thin disks behave in a brittle manner. Both the Tresca yield condition

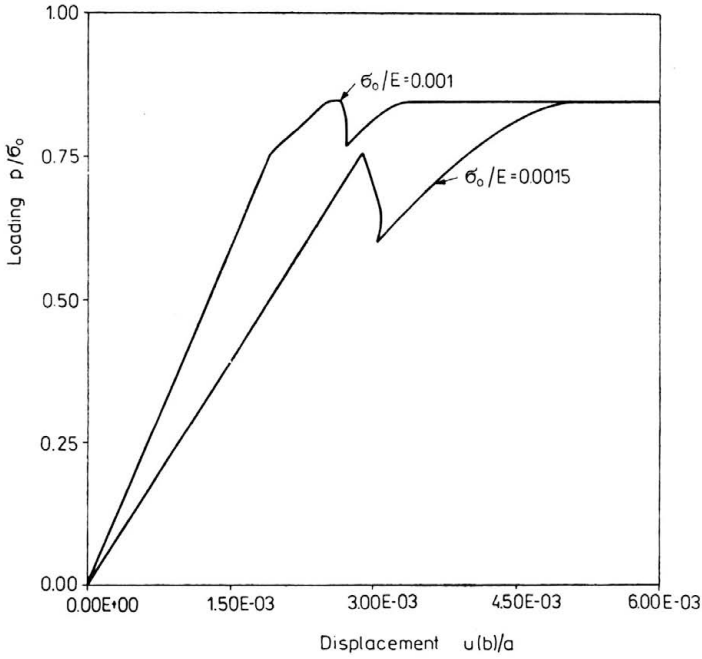

FIG. 13. Effect of Young's modulus on load-displacement curves for the Huber–Mises yield condition and the deformation theory.
Disk parameters: $b/a = 4$, $a/H = 250$, $\nu = 0.3$.

and the deformation theory predict similar responses. Figures 12 and 13 illustrate the effect of varying Poisson ratio and Young's modulus. It is seen that the decohesion stress and elasto-plastic response depend on the elastic moduli.

5. Concluding remarks

The present paper, though concerned with a simple example, presents a method for solving elasto-plastic problems taking into account post-critical states. Since the large deformation process is confined to a narrow cohesive zone, its effect on the whole structure

is described by formulating a constitutive relation between the respective traction and displacement discontinuities or their rates. A complex character of plastic deformation is demonstrated in the analysis. A primary plastic zone is followed by unloading, and a secondary plastic zone appears near the edge and propagates throughout the whole disk.

The present analysis also indicates that the assumption of brittle decohesion used by SZUWALSKI and ŻYCZKOWSKI in [3–9] may not be justified in all cases. According to the conclusions reached in [3–9], brittle decohesion occurs independently of disk thickness once the stress point has reached the parabolic regime S_1 on the yield surface and the disk is fully elastic at this state. The subsequent elasto-plastic deformation process occurs after the separation of disk and hub. However, the present analysis provides different conclusions.

Depending on disk thickness, at the state of decohesion the disk may be in elastic or elasto-plastic stress regimes. The size of the plastic zone near the edge $r = a$ increases with disk thickness. As it follows from Fig. 12, the value of the Poisson ratio ν does not affect the load value corresponding to the end of decohesion but affects the value of displacements of external edge $r = b$.

In general, the onset of decohesion may be followed by both stable or unstable response, so the complete elasto-plastic analysis should be carried out in order to describe the structural response. Disk thickness H is very essential in this analysis since the decohesive ductility specified by the conditions (2.21) depends explicitly on H. As it follows from Figs. 10 and 11, the load-displacement curves are much dependent on the ratio a/H.

The present analysis and method may be generalized to more complex loading cases involving both extension and flexure, and also to nonaxisymmetric cases. These cases are now being studied within the set of assumptions outlined in the paper.

Appendix

To assess the error introduced by assumption of stress homogeneity near the edge $r = a$, consider the elastic stress state. From Eqs. (2.4) and (3.2) it follows that

$$\frac{\sigma_r\left(a+\frac{H}{2}\right)}{\sigma_r(a)} = \frac{1}{2}\left[1+\nu+(1-\nu)\frac{a^2}{\left(a+\frac{H}{2}\right)^2}\right],$$

$$\frac{\sigma_t\left(a+\frac{H}{2}\right)}{\sigma_t(a)} = \frac{1}{2\nu}\left[1+\nu-(1-\nu)\frac{a^2}{\left(a+\frac{H}{2}\right)^2}\right]$$

and since $H \ll a$, there is $\sigma_r\left(a+\frac{H}{2}\right) \approx \sigma_r(a)$ and $\sigma_t\left(a+\frac{H}{2}\right) \approx \sigma_t(a)$. The departure from homogeneity did not exceed 0.5% in the examples presented.

When the primary plastic zone exists before the decohesion process, then, depending on ν and H, the decohesive zone may lie totally or partially within the plastic zone. Assuming that for a sufficiently thin disk the decohesive zone lies within the plastic zone, then

the stress profile near $r = a$ would lie on the yield curve in Fig. 2 between A and S_1. Hence the maximal difference between $\sigma_r\left(a+\frac{H}{2}\right)$ and $\sigma_r(a)$ cannot exceed 17%.

The derivation of Eqs. (2.20) follows the assumption of the plain strain state. For the axisymmetric case, the slip lines would not be straight, cf. [10]. However, the error involved with our approximation is insignificant for relatively thin disks (small values of H/a). Moreover, any other relation between $\sigma_r(A'A'')$ and u_d could be used in the analysis without any conceptual difficulties.

References

1. E. M. SHOEMAKER, *Some paradoxes with elastic-plastic limit load analysis*, Arch. Mech., **20**, 4, pp. 473–483, 1968.
2. J. LENARD, J. B. HADDOW, *Plastic collapse speeds for rotating cylinder*, Int. J. Mech. Sci., **14**, pp. 285–292, 1972.
3. K. SZUWALSKI, M. ŻYCZKOWSKI, *On the phenomenon of decohesion in perfect plasticity*, Int. J. Solids Struct., **9**, 1, pp. 85–98, 1973.
4. K. SZUWALSKI, *Decohesive carrying capacity of annular axially-symmetrical disc with rigid inclusion*, Mech. Teor. Stos., **17**, 4, pp. 589–602, 1979 [in Polish].
5. K. SZUWALSKI, *Influence of material characteristic on decohesive carrying capacity of an infinite plate with a circular rigid inclusion*, Ing. Trans., **33**, 1–2, pp. 55–69, 1985 [in Polish].
6. K. SZUWALSKI, *Perfectly elastic-plastic hyperbolic disk*, Mech. Teor. Stos., **22**, 3–4, pp. 539–547, 1984 [in Polish].
7. K. SZUWALSKI, *The limit and decohesive load-carrying capacity of a rotating disc of jump-like nonhomogeneity*, Arch. Bud. Masz., **32**, 1–2, pp. 53–66, 1985 [in Polish].
8. K. SZUWALSKI, M. ŻYCZKOWSKI, *A concave interaction curve corresponding to decohesive carrying capacity under thermal loading*, J. Thermal Stress., **7**, 121–134, 1984.
9. M. ŻYCZKOWSKI, K. SZUWALSKI, *On the termination of the process of finite plastic deformations*, J. de Mech., 175–186, 1982.
10. W. SZCZEPIŃSKI, *Introduction to the mechanics of plastic forming of metals*, PWN, Warszawa 1967 [in Polish].

POLISH ACADEMY OF SCIENCES
INSTITUTE OF FUNDAMENTAL TECHNOLOGICAL RESEARCH.

Received November 4, 1987.